Available online at www.sciencedirect.com
ScienceDirect
Trans. Nonferrous Met. Soc. China 28(2018) 676−686
Transactions of Nonferrous Metals Society of China
www.tnmsc.cn

Facile synthesis of 3D nanoporous Pd/Co_2O_3 composites with enhanced catalytic performance for methanol oxidation

Yan-yan SONG[1,2,3], Dong DUAN[1,2,3], Wen-yu SHI[1,2,3], Hai-yang WANG[1,2,3], Zhan-bo SUN[1,2,3]

1. School of Science, Xi'an Jiaotong University, Xi'an 710049, China;
2. Key Laboratory for Non-Equilibrium Synthesis and Modulation of Condensed Matter of Ministry of Education, Xi'an Jiaotong University, Xi'an 710049, China;
3. Key Laboratory of Shaanxi for Advanced Functional Materials and Mesoscopic Physics, Xi'an Jiaotong University, Xi'an 710049, China

Received 8 November 2016; accepted 27 May 2017

Abstract: To simultaneously reduce noble metal Pd usage and enhance electrocatalytic performance for methanol oxidation, Pd/Co_2O_3 composites with ultrafine three-dimensional (3D) nanoporous structures were designed and synthesized by simple one-step dealloying of a melt-spun Al−Pd−Co alloy with an alkaline solution. Their electrocatalytic activity in alkaline media was determined by a Versa-STAT MC workstation. The results indicate that the typical sizes of the ligaments and pores of the composites were approximately 8−9 nm. The Co_2O_3 was uniformly distributed on the Pd ligament surface. Among the as-prepared samples, the nanoporous Pd/Co_2O_3 composite generated from dealloying of the $Al_{84.5}Pd_{15}Co_{0.5}$ alloy had the best electrocatalytic activity, and its activity was enhanced by approximately 230% compared with the nanoporous Pd from dealloying of $Al_{85}Pd_{15}$. The improvement of the electrocatalytic performance was mainly attributed to the electronic modification effect between Pd and Co as well as the bifunctional mechanism between Pd and Co_2O_3.

Key words: nanoporous Pd/Co_2O_3; dealloying; Al−Pd−Co alloy; electrocatalytic performance; methanol oxidation

1 Introduction

Recently, nanoporous (np) noble metals, such as np Pt [1,2] and np Au [3,4], have attracted considerable attention due to their large surface area, ultralow density, cost reduction, excellent electrical and thermal conductivities, and catalytic recyclability [5,6], which hold great promise for electrocatalysis [7−9], sensing [10,11], energy storage devices [12], and fuel cells [13]. The dealloying method in previous reports has been demonstrated to be a powerful and facile method to prepare nanoporous metallic materials [14−16]. During this process, the reactive atomic content in source alloys can be controlled to be a suitable level, and then, the source alloys can be etched through chemical or electrochemical methods to selectively dissolve one or more components from the alloy, leading to the formation of a bicontinuous open nanoporous structure [6,17,18].

It is well known that catalysis at the electrode is a surface phenomenon and that the catalytic activity depends on the dispersion or exposed percentage of active atoms in the catalyst [19]. Therefore, the design of hybrids that contain more active atoms on the outer surface of the material is being pursued to make the most efficient use of noble metals [20]. For now, loading noble metal nanoparticles on different transition metal oxide supporting materials is a conventional synthesis strategy [21,22]. Unfortunately, these noble metal-based catalysts are prone to noble metal particle agglomeration and their stability becomes poor during long-term catalysis. Therefore, catalysts are generally subjected to a poison that is generated from carbon monoxide adsorption during the catalytic process, resulting in lower utilization of noble metals and reduction of the catalytic efficiency [23]. Moreover, oxide supports, such as semiconductors, will lead to a performance decline due to the reduction of the conductivity of the electrocatalyst.

However, what would happen if nanoporous noble

Foundation item: Project (51371135) supported by the National Natural Science Foundation of China
Corresponding author: Zhan-bo SUN; Tel/Fax: +86-29-82665995; E-mail: szb@mail.xjtu.edu.cn
DOI: 10.1016/S1003-6326(18)64700-4

metals are used as supporting materials and transition metal oxides are used as promoters to decrease the utilization of noble metals? Nanoporous noble metals with three-dimensional (3D) bicontinuous interpenetrating structures have high structural stability with no agglomeration. This feature allows nanoporous noble metal supporting materials to not only minimize the amount of noble metal used, reduce the cost and result in full utilization of noble metals, but also enable the maximum exposure of active sites, leading to absorption of small organic molecules in the electrolyte, providing a short transportation path for electrons and ions, and generating faster reaction kinetics and higher electrocatalytic reactivity [24]. Furthermore, noble metals that have outstanding electron conductivity can serve as electronic conductive supports and facilitate electron transfer, which would lead to a high electrocatalytic performance. If a transition metal oxide is used as a promoter on the surface of a np noble metal, oxygen-containing species (OH_{ads}) can form more easily, so the interaction between the np noble metal and transition metal oxide would be more efficient. In a series of previous studies, we have demonstrated that composites designed for the above strategy possess outstanding catalytic activity, including the Ag−MO_2 (M=Ce, Ti, Zr) catalyst [25−27].

Among the np noble metals, nanoporous Pd is of special interest due to its relative abundance in nature, low cost, and good resistance to CO poisoning, which has caused it to have been widely used as a superior catalyst for a variety of research fields ranging from organic synthesis and fuel cells to environmental protection [28−30]. Thus, in the present work, 3D np-Pd/Co_2O_3 composites with a controllable composition were fabricated through one-step dealloying of a ternary Al−Pd−Co alloy in an alkaline solution, which has not been previously reported.

2 Experimental

2.1 Preparation of nanoporous composites

Al−Pd−Co alloys were produced by arc-melting pure elements (Al: 99.9%, Pd: 99.9%, Co: 99.9%) in a high-frequency induction furnace in a pure argon atmosphere. This process yielded alloys with nominal compositions of $Al_{85-x}Pd_{15}Co_x$ (x=0, 0.3, 0.5, 0.7, 1). From the alloys, ribbons with a thickness of 30 μm and width of 3 mm were fabricated using the melt-spinning method under a pure argon atmosphere as reported in our previous work [31]. Ribbon dealloying was performed in an aqueous 20% (mass fraction) NaOH solution at 60 °C for 48 h. The dealloyed ribbons were rinsed with distilled water, dried at 50 °C in a drying oven, and then stored in a vacuum chamber prior to further testing. Note that the reaction rate increased with increasing concentrations of NaOH solution, but excessive concentrations resulted in an undesirable coarsening of the ligaments [32]. Experiments have shown that 20% (mass fraction) NaOH can be used to dealloy Al−Pd based alloys.

2.2 Characterization

The structures, morphologies and compositions of all samples were characterized by a Bruker D8 advanced X-ray diffractometer (XRD), JEM−2100 high-resolution transmission electron microscope (HRTEM, JEOL Ltd.), Fei Titan Themis 200 TEM, a JSM−7000F scanning electron microscope (SEM, JEOL Ltd.) equipped with an energy disperse spectroscope (EDS), and axis Ulra Kratos X-ray photoelectron spectrometer (XPS) using an Al K_α X-ray source (1486.68 eV).

2.3 Electrochemical measurements

A Versa-STAT MC workstation with a classical three-electrode cell was used for the electrochemical measurements. The preparation process of the working electrode was as follows: First, 2 mg of a finely-ground dealloyed sample and 0.5 mg of an acetylene black were dispersed in a mixing solution of 200 μL of isopropanol and 200 μL of Nafion (0.5%, mass fraction) to form an evenly distributed catalyst suspension liquid by sonication. Then, 2 μL of the suspension liquid was spread on a polished glassy carbon electrode (GC) that had a geometric area of 0.071 cm^2 (which acted as the working electrode), and finally, the electrode was dried at room temperature in air. A platinum net (1 cm^2) and Ag/AgCl (saturated KCl) electrode served as the counter electrode and reference electrode, respectively. The electrocatalytic activity and stability of the dealloyed samples for methanol oxidation were measured in 0.5 mol/L CH_3OH and 0.5 mol/L KOH. The electrolyte solutions were deaerated with ultrahigh purity nitrogen for 30 min prior to any measurement. All of the electrochemical experiments were conducted at ambient temperature.

3 Results and discussion

3.1 Microstructural characterization of np-Pd/Co_2O_3 composites

The XRD patterns of the dealloyed Al−Pd and the Al−Pd−Co samples are presented in Fig. 1. It can be seen that only the diffraction peaks of fcc-Pd (PDF #46−1043) were detected in the dealloyed Al−Pd sample, and no additional diffraction peaks related to Al (or its oxides) were observed. The pattern of the dealloyed Al−Pd−Co was similar to that of the dealloyed Al−Pd sample, and the diffraction peaks of pure Co or its oxides could not be readily detected. The broadness of the diffraction

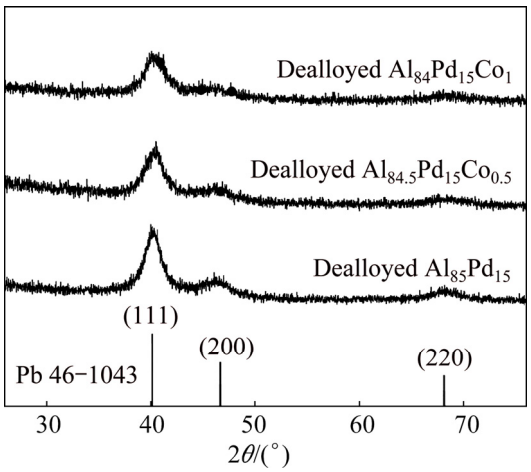

Fig. 1 XRD patterns of dealloyed $Al_{85-x}Pd_{15}Co_x$ (x=0, 0.5, 1) ribbons

peaks in all the samples may arise from the large surface strain that formed during dealloying because of the smaller ligament size and smaller grain size.

Figure 2 illustrates representative SEM and EDS images of the dealloyed Al−Pd and Al−Pd−Co samples. From the plane-section and cross-section images, as shown in Figs. 2(a) and (b), a typical bicontinuous nanoporous structure with ultrafine nanoscale ligaments and open pores was successfully generated, and interconnected hollow channels extended throughout the sample, indicating that the dealloyed Al−Pd sample had a 3D nanoporous structure. After adding a certain amount of Co to the precursor alloy, as shown in Figs. 2(c)−(f), the micromorphology and structure of the dealloyed Al−Pd−Co samples maintained an excellent 3D nanoporous structure. However, with the addition of a very small amount of Co, the nanoporous structure of

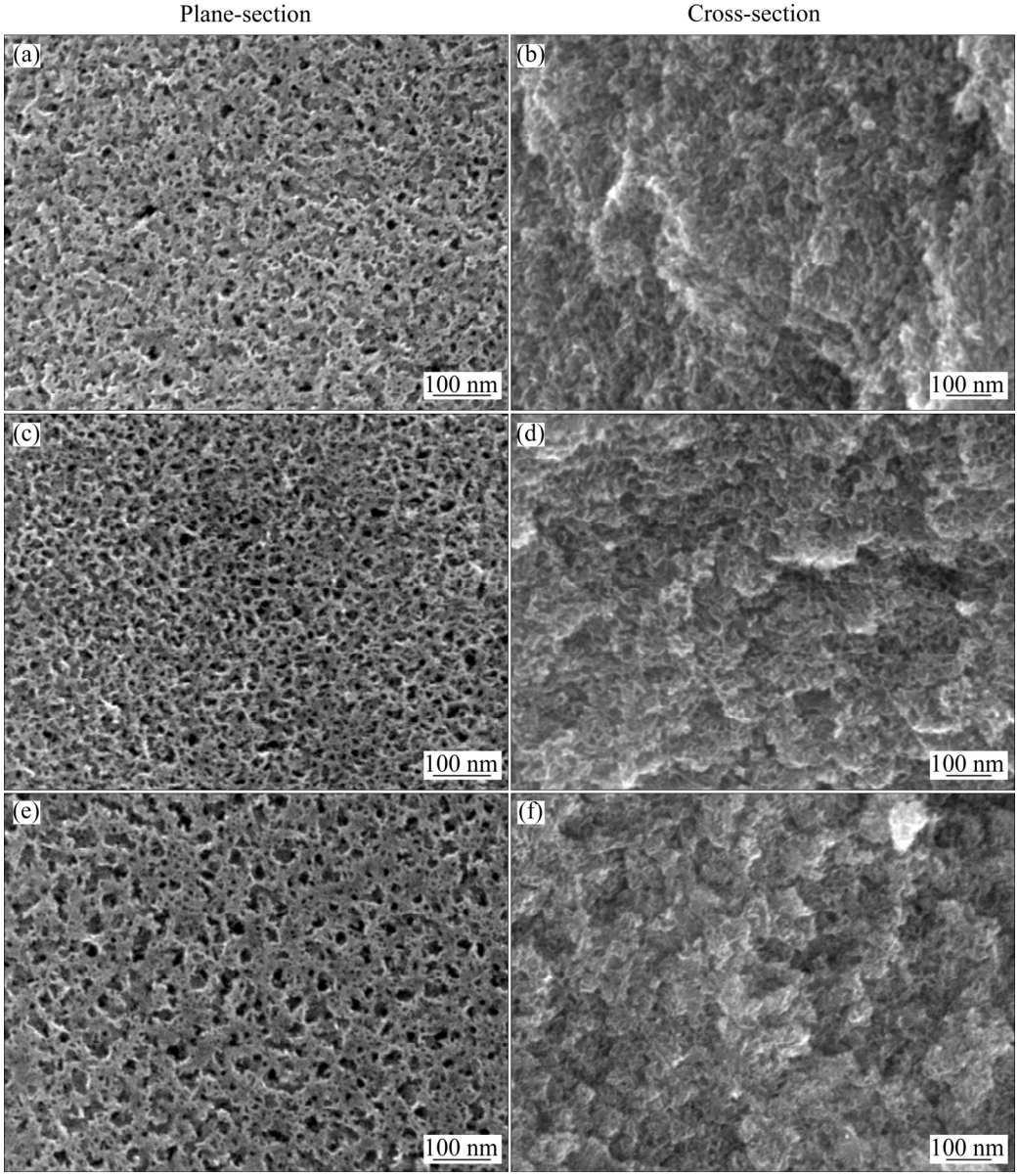

Fig. 2 SEM images showing typical microstructures of dealloyed ribbons: (a, b) $Al_{85}Pd_{15}$; (c, d) $Al_{84.5}Pd_{15}Co_{0.5}$; (e, f) $Al_{84}Pd_{15}Co_1$

the dealloyed $Al_{84.5}Pd_{15}Co_{0.5}$ sample exhibited a refinement phenomenon (Figs. 2(c) and (d)) compared with the dealloyed Al−Pd. This may lead to a larger electrochemically-active surface area, and may produce more active sites for the electrocatalytic process. As the amount of Co is further increased (Figs. 2(e) and (f)), the nanoporous structure of the dealloyed $Al_{84}Pd_{15}Co_1$ becomes coarser.

The typical EDS pattern and resulting data of the dealloyed Al−Pd−Co samples are shown in Fig. 3 and Table 1. The results indicate that the dealloyed ribbons were mainly composed of Pd, Co, O and residual Al. Most of the Al atoms were removed during the dealloying process. The Pd and Co contents (experimental values) were basically consistent with the initial feeding ratios of Pd to Co in the ternary Al−Pd−Co alloy (theoretical values). This illustrates that the composition of the resulting sample was well controlled by the dealloying method. Considering that the Co content is low in the composites, the related diffraction peaks are hard to be detected by XRD.

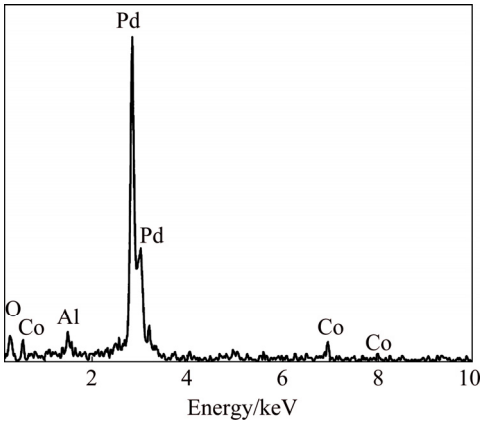

Fig. 3 Typical EDS pattern of dealloyed $Al_{84}Pd_{15}Co_1$ ribbon

The BET surface areas and mean pore diameters of the dealloyed $Al_{85-x}Pd_{15}Co_x$ (x=0, 0.3, 0.5, 0.7, 1) samples are provided in Table 2. It can be seen that with the addition of elemental Co to the precursor alloy, the surface areas and pore volumes of the dealloyed Al−Pd−Co samples became noticeably larger and their mean pore diameters became distinctly smaller than those of the dealloyed $Al_{85}Pd_{15}$ sample. Furthermore, it should be noted that when the Co content is too great (x>0.5), the surface areas and pore volumes of the dealloyed Al−Pd−Co samples will be reduced and their pore sizes will be increased. That is to say, the nanoporous structures of the dealloyed $Al_{84.3}Pd_{15}Co_{0.7}$ and $Al_{84}Pd_{15}Co_1$ samples present a coarsening trend, which is consistent with the SEM images (Fig. 2). This represents an adverse phenomenon for catalytic activity toward methanol oxidation. Therefore, the dealloyed $Al_{84.5}Pd_{15}Co_{0.5}$ sample had the best morphology.

The TEM and HRTEM images and corresponding selected area electron diffraction (SAED) pattern of the dealloyed $Al_{84.5}Pd_{15}Co_{0.5}$ sample, as representative of a typical pattern for the dealloyed Al−Pd−Co samples, are shown in Fig. 4. The results demonstrate that the ligaments of the dealloyed sample interconnect with each other and that a bicontinuous ligament-channel structure is generated, which is in agreement with the SEM observation. The SAED and HRTEM images indicate that the samples possess a polycrystalline structure that is composed of randomly oriented fcc Pd and that one of the lattice fringe spacings is 0.224 nm, which is consistent with the distance of the dominant (111) planes for Pd. The typical sizes of the ligaments and pores are approximately 8−9 nm.

The elemental distribution of the nanoporous structure from the dealloyed $Al_{84.5}Pd_{15}Co_{0.5}$ sample is

Table 1 EDS data results of dealloyed $Al_{85-x}Pd_{15}Co_x$ (x= 0.3, 0.5, 0.7, 1) ribbons

Dealloyed ribbon	x(Pd)/%	x(Co)/%	x(Al)/%	x(Pd):x(Co)	
				Theoretical	Experimental
$Al_{84.7}Pd_{15}Co_{0.3}$	89.25	2.03	8.72	98.04:1.96	97.78:2.22
$Al_{84.5}Pd_{15}Co_{0.5}$	88.41	3.16	8.43	96.77:3.23	96.55:3.45
$Al_{84.3}Pd_{15}Co_{0.7}$	87.84	3.91	8.25	95.54:4.46	95.74:4.26
$Al_{84}Pd_{15}Co_1$	85.29	5.75	8.96	93.75:6.25	93.68:6.32

Table 2 BET surface areas and mean pore diameters of dealloyed $Al_{85-x}Pd_{15}Co_x$ (x=0, 0.3, 0.5, 0.7, 1) ribbons

Dealloyed ribbon	Surface area/($m^2 \cdot g^{-1}$)	Pore diameter/nm	Pore volume/($cm^3 \cdot g^{-1}$)
$Al_{85}Pd_{15}$	40.288	10.082	0.102
$Al_{84.7}Pd_{15}Co_{0.3}$	52.460	8.825	0.116
$Al_{84.5}Pd_{15}Co_{0.5}$	58.196	8.555	0.124
$Al_{84.3}Pd_{15}Co_{0.7}$	54.961	8.869	0.122
$Al_{84}Pd_{15}Co_1$	54.557	8.821	0.120

provided by TEM−EDS mapping. From Fig. 5, the dealloyed samples are mainly composed of Pd, Co and O. By combining Fig. 4 and Fig. 5, the results indicate that the ligaments in the nanoporous structure are composed of Pd atoms, as shown in Fig. 5(b) and that the Co and O atoms are uniformly distributed on the ligament surfaces of the nanoporous structure, as shown in Figs. 5(c) and 5(d).

The surface compositions of the dealloyed Al−Pd−Co ribbons were determined by XPS. The spectra of Pd 3d and Co 2p are shown in Fig. 6, and their related splitting spectra were also collected to determine the valence states of Pd and Co. Both Pd and PdO peaks are present on the surface of the dealloyed sample, as seen in Fig. 6(a). The Pd $3d_{5/2}$ peak at 335.4 eV and $3d_{3/2}$ peak at 340.4 eV are attributed to metallic Pd (Pd^0) [33,34]. The doublet peaks located at 336.3 and 342.4 eV are assigned to PdO (Pd^{2+}) according to Refs. [35,36], indicating that a small amount of PdO is generated during the dealloying process. Compared with the Pd 3d spectrum of the dealloyed $Al_{85}Pd_{15}$ [31], the Pd 3d spectrum of the dealloyed $Al_{84.5}Pd_{15}Co_{0.5}$ ribbons presents a slightly negative shift to a lower binding energy. In addition, it should be noted that the form of the Co atoms on the ligament surfaces of the samples is Co_2O_3 and no metallic Co (Co^0) is found, as shown in Fig. 6(b). This is

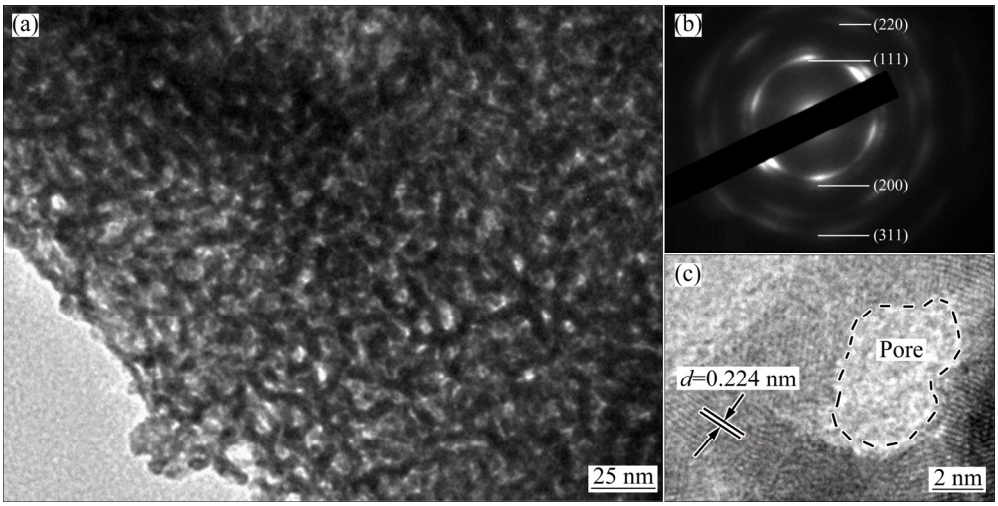

Fig. 4 TEM image of dealloyed $Al_{84.5}Pd_{15}Co_{0.5}$ ribbons (a), corresponding SAED pattern (b), and HRTEM image (c)

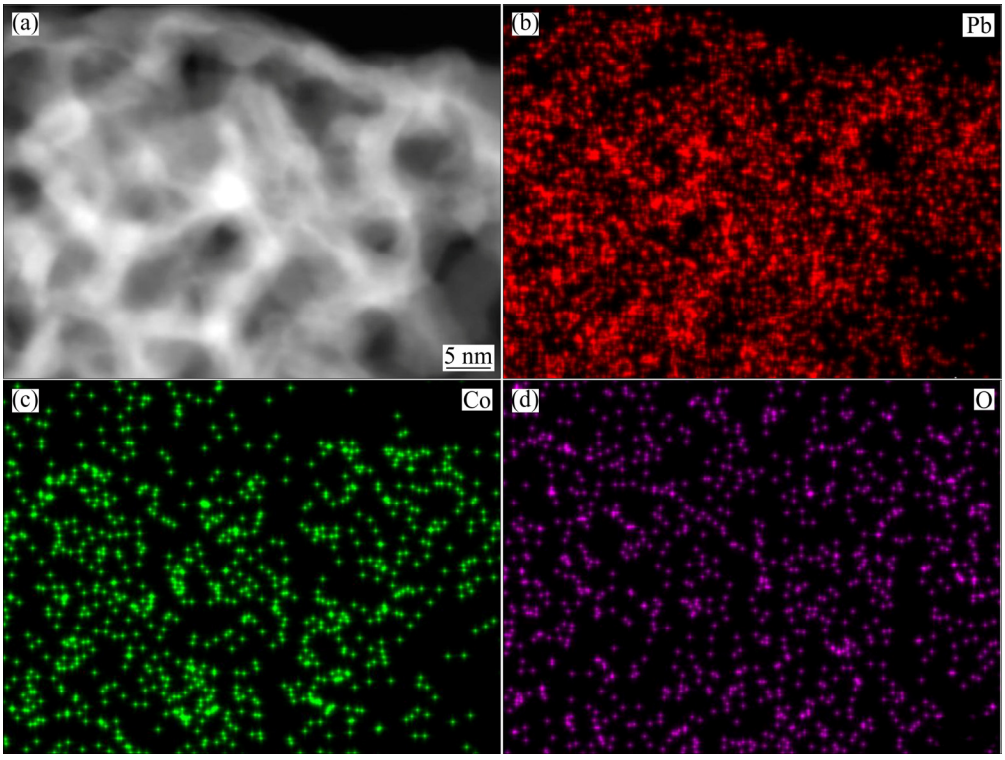

Fig. 5 TEM image (a) of dealloyed $Al_{84.5}Pd_{15}Co_{0.5}$ ribbons and corresponding EDS element mapping of Pd (b), Co (c) and O (d)

due to the fact that the primary peaks located at 781.3 eV and 797.1 eV in the Co 2p orbital belong to Co $2p_{3/2}$ and Co $2p_{1/2}$ of Co_2O_3, respectively, according to Ref. [37]. The peaks located at 787.6 eV and 804.8 eV are their corresponding satellite signals.

The above results reveal that np-Pd/Co_2O_3 composites were fabricated by simple one-step dealloying of the ternary Al−Pd−Co precursor alloy. The composites possess a 3D nanoporous structure, and their compositions can be controlled well. The formation mechanism is shown in Fig. 7. Because Al is leached away, the remaining Pd and Co atoms can interdiffuse at the solution/solid interface and self-assemble to form 3D bicontinuous nanoporous structures. Meanwhile, highly active Co atoms undergo natural oxidation in aqueous solutions over an extended period of time (48 h) to form Co_2O_3. The formation process of Co_2O_3 is similar to that reported in Ref. [38]. As a result, 3D np-Pd/Co_2O_3 samples are formed.

3.2 Electrocatalytic performance of np-Pd/Co_2O_3 composites

For convenience, the dealloyed $Al_{85}Pd_{15}$, $Al_{84.7}Pd_{15}Co_{0.3}$, $Al_{84.5}Pd_{15}Co_{0.5}$, $Al_{84.3}Pd_{15}Co_{0.7}$ and $Al_{84}Pd_{15}Co_1$ ribbons are designated as np-Pd, np-Pd/Co_2O_3-1, np-Pd/Co_2O_3-2, np-Pd/Co_2O_3-3 and np-Pd/Co_2O_3-4, respectively.

As seen in Fig. 8, background cyclic voltammograms (CVs) of the samples were collected in a 0.5 mol/L KOH solution at a scan rate of 20 mV/s. The typical CV profiles of the np-Pd/Co_2O_3 composites are similar to those of np-Pd [31]. Pd oxides are formed on the surface of the composites at the high potential end during the positive sweep, leading to a reduction of the characteristic peak at approximately −0.37 V during the negative scan (Fig. 8(a)) [39,40]. The electrochemically active surface area (EASA) of a noble metal is usually used to evaluate the number of catalytically-active sites. Generally, the EASA of Pd or Pd-based catalysts can be estimated according to the following equation 1 [41]:

$$A = \frac{Q_s}{Q_c m} \tag{1}$$

where Q_s is the coulombic charge (μC) obtained by integrating the current peak of Pd oxide reduction, Q_c is the conversion factor and is commonly taken as 405 μC/cm^2, and m is the mass (mg) of Pd. Though the measurement of EASA in alkaline media may deviate

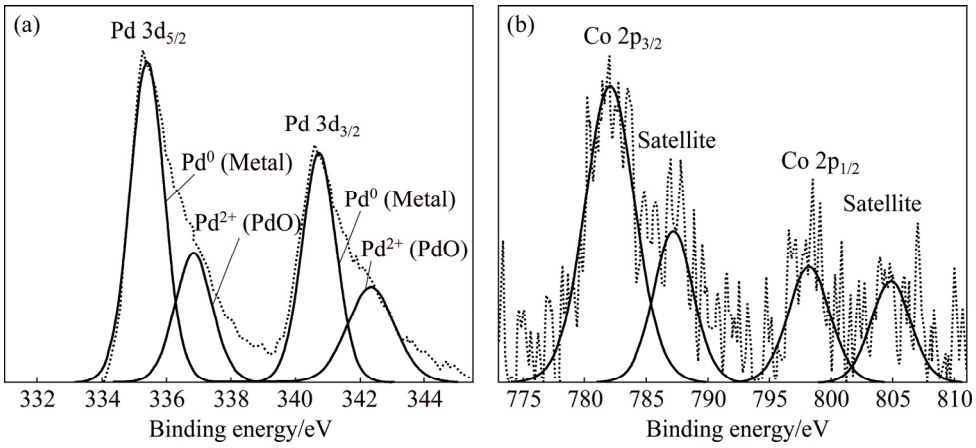

Fig. 6 XPS spectra of Pd 3d (a) and Co 2p (b) of dealloyed $Al_{84.5}Pd_{15}Co_{0.5}$ ribbons

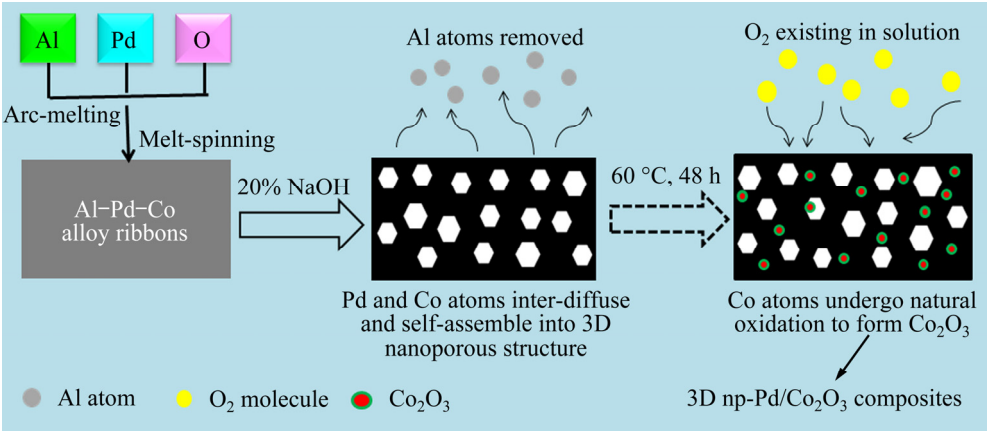

Fig. 7 Formation mechanism of 3D np-Pd/Co_2O_3 composites

from the true value because complex oxide multilayer rather than a monolayer is present on the surface of Pd, it can be used when comparing a series under identical conditions. The EASAs of np-Pd, np-Pd/Co_2O_3-1, np-Pd/Co_2O_3-2, np-Pd/Co_2O_3-3 and np-Pd/Co_2O_3-4 composites are 52.0, 56.2, 78.9, 72.9 and 65.1 m^2/g, respectively, as shown in Fig. 8(b). The EASA gradually increases with the increase in Co_2O_3 content and then decreases with a further increase in Co_2O_3 content. The EASA value of the np-Pd/Co_2O_3 composites is all higher than that of the np-Pd.

Figure 9 shows the CVs of np-Pd/Co_2O_3 and np-Pd in 0.5 mol/L KOH + 0.5 mol/L methanol. The oxidation peak can be assigned to the oxidation of a freshly-chemisorbed species that comes from methanol adsorption. The peak current densities (J_p) of methanol

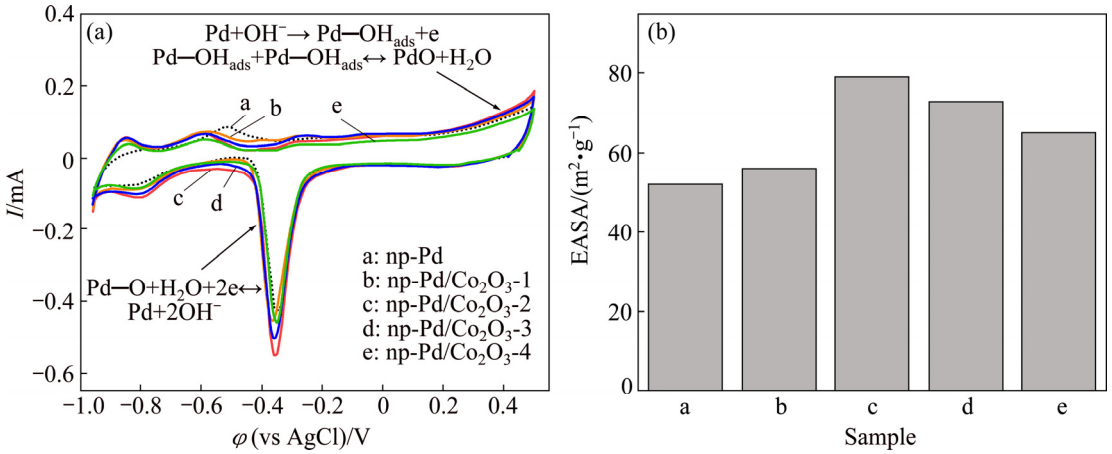

Fig. 8 CV curves of np-Pd and np-Pd/Co_2O_3 composites in 0.5 mol/L KOH solution at scan rate of 20 mV/s (a) and corresponding calculated EASA values of samples (b)

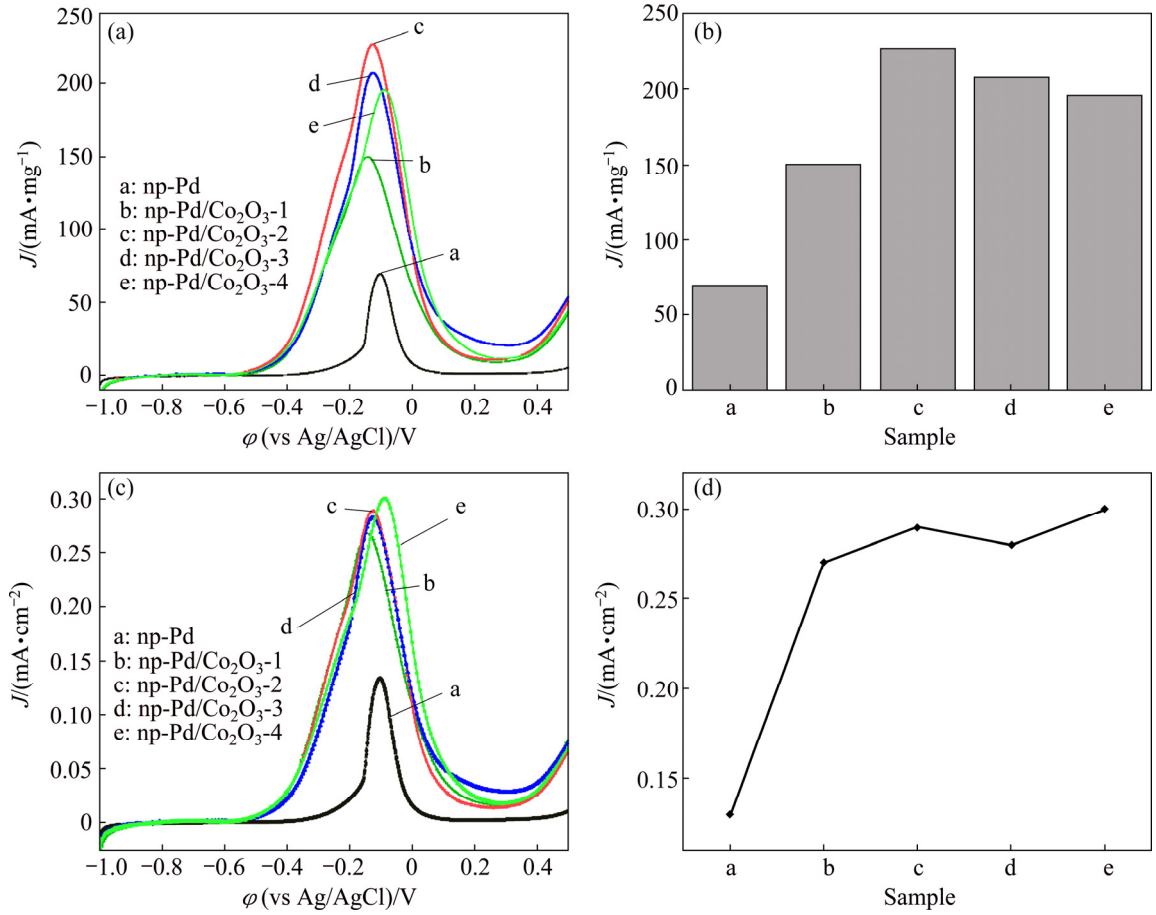

Fig. 9 CV curves of np-Pd and np-Pd/Co_2O_3 composites in 0.5 mol/L KOH + 0.5 mol/L methanol solution at scan rate of 20 mV/s: (a, b) Mass specific current and corresponding peak current; (c, d) Surface specific current and corresponding peak current

oxidation are regarded as primary parameters to evaluate the electrocatalytic activities of the catalysts [42]. The catalytic activity of the composites is evaluated by the mass-normalized current density, which intuitively reflects the synergistic effect between Co_2O_3 and Pd, as shown in Fig. 9(a). The calculated mass activities (J_p^{mass}) of the np-Pd/Co_2O_3-1, np-Pd/Co_2O_3-2, np-Pd/Co_2O_3-3 and np-Pd/Co_2O_3-4 composites reach 150.3, 227.2, 207.2 and 195.8 mA/mg, respectively, as shown in Fig. 9(b). By comparison, these activities are 2.2, 3.3, 3.0 and 2.8 times that of np-Pd (69.7 mA/mg), respectively. Thus, all of the composites have higher electrocatalytic performances than np-Pd, and np-Pd/Co_2O_3-2 has the best activity for methanol oxidation. Simultaneously, the EASA normalized current density is also examined for all samples to further compare their intrinsic activity, as shown in Fig. 9(c). The J_p^{EASA} of the np-Pd/Co_2O_3 composites in the methanol solution is at least twice as large as that of np-Pd, as shown in Fig. 9(d). In addition, regarding the onset potential (φ_{op}), np-Pd/Co_2O_3 composites possess more negative φ_{op} values compared with np-Pd. The values of φ_{op} for np-Pd/Co_2O_3 composites are similar (approximately −0.55 V), which is approximately 0.2 V less than that of np-Pd (approximately −0.35 V), as indicated by the arrows in Fig. 9. This result demonstrates that the np-Pd/Co_2O_3 composites require a lower potential than np-Pd catalysts to perform methanol oxidation, that is, electrocatalytic methanol oxidation occurs more easily [43].

The long-term stability of electrocatalysts for methanol oxidation is further investigated according to the chronopotentiometric (CA) curves in a solution of 0.5 mol/L KOH + 0.5 mol/L CH_3OH at −0.14 V vs Ag/AgCl. Figure 10 shows the CA curves normalized by the equivalent mass of Pd (J^{mass}) and EASA (J^{EASA}) for the samples. The initial current density drops according to the carbonaceous intermediates generated on the surface of the electrode during methanol oxidation [44]. The CA curves indicate that all of the np-Pd/Co_2O_3 composites are more durable than np-Pd, which can be attributed to the minimization of the accumulation of poisoning species on the Pd active sites by the addition of Co_2O_3. In sum, the np-Pd/Co_2O_3-2 composite has the optimum electrocatalytic performance and stability for methanol oxidation, which means that the np-Pd/Co_2O_3-2 composite achieves a balance between catalytic activity and poison resistance when the appropriate form of Co_2O_3 is used. Additionally, the order of the stabilities of the samples for methanol oxidation is in good agreement with the CV results.

The transportation characteristics of the np-Pd/Co_2O_3-2 composite were investigated by varying the scan rate in 0.5 mol/L KOH and 0.5 mol/L CH_3OH solutions, and the results are shown in Fig. 11. J^{mass} increases with the increasing scan rate, as shown in Fig. 11(a), indicating that the electrocatalytic oxidation of methanol on the composites may be a diffusion-controlled process. The relationship between J^{mass} and $v^{1/2}$ is linear (Fig. 11(b)), confirming that the electrocatalytic oxidation of methanol on np-Pd/Co_2O_3-2 is a diffusion-controlled process [45,46]. Additionally, the peak potential (φ_p) increases with the increase of v, and a linear relationship is obtained between φ_p and ln v, as shown in Fig. 11(c). This indicates that the oxidation of methanol on the np-Pd/Co_2O_3-2 composite is an irreversible electrode process [41].

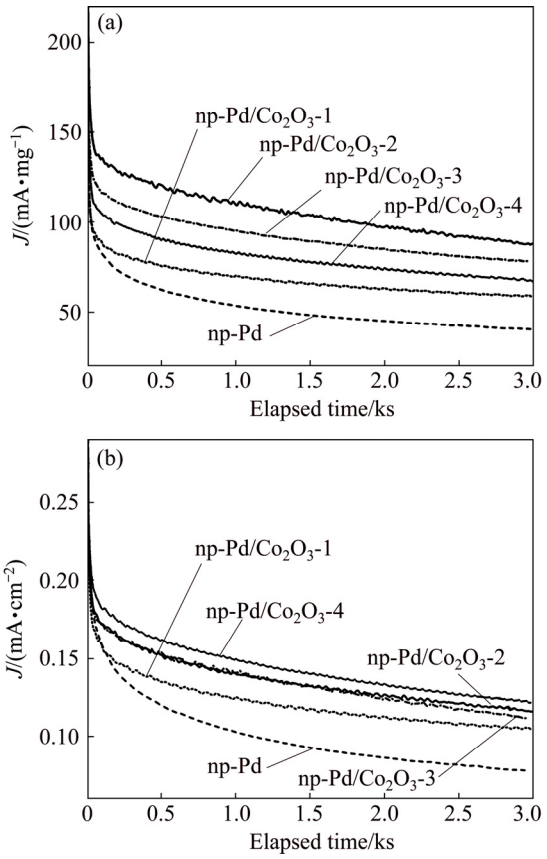

Fig. 10 Chronopotentiometric curves of 0.5 mol/L methanol in 0.5 mol/L KOH solution on np-Pd/Co_2O_3 and np-Pd samples at potential of −0.14 V vs Ag/AgCl: (a) Mass specific current; (b) Surface specific current

According to the experimental results, np-Pd/Co_2O_3 composites have excellent electrochemical activity, long-term stability and low φ_{op}. The primary reasons that the components have these properties can be rationalized as follows. First, an electronic modification effect is present between Pd and Co. After adding Co to the precursor alloy, the XPS peaks of Pd 3d undergo a slightly negative shift to lower binding energies compared with those of np-Pd (Fig. 6). The negative shift of the Pd peaks in the composites is due to the small

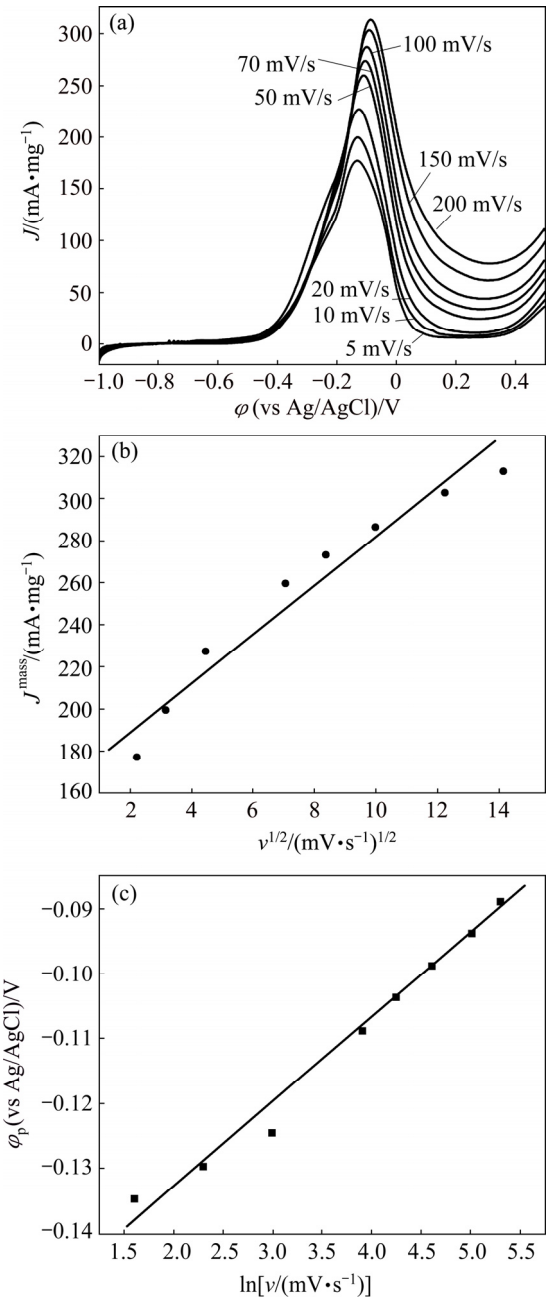

Fig. 11 CV curves of 0.5 mol/L methanol in 0.5 mol/L KOH solution on np-Pd/Co_2O_3-2 composite: (a) At different scan rates; (b) J^{mass} vs $v^{1/2}$; (c) φ_p vs ln v

electron transfer from Co to Pd because the electronegativity of Co (1.88) is much smaller than that of Pd (2.2) [47], which indicates that the addition of Co to the precursor alloy modifies the electronic structure of Pd and produces an electronic modification effect between Pd and Co. In addition, electron transfer can influence the d-band density of Pd. According to previous research [47,48], the Pd d-band center will shift to a lower energy after adding Co to Pd, resulting in weaker Pd-adsorbate bonds, that is to say, the adsorption of the adsorbates is weaker at the Pd sites. In this way, Pd poisoning by CO-like species is decreased because these species are more weakly adsorbed on Pd, and more Pd sites are released for continuous methanol oxidation, which leads to enhancement of the activity. Second, there is a bifunctional mechanism between Pd and Co_2O_3. As some intermediates, especially CO, are formed at Pd active sites, some intermediates accumulate on the active sites surface, blocking adsorption of methanol molecules. Therefore, catalytic activation is restricted. The addition of Co to the precursor can effectively relieve the above problem because the Co atoms in the precursor alloy are completely oxidized into Co_2O_3 after undergoing the extensive dealloying process. Co_2O_3 can provide the necessary OH species, which are permanently be available at the Co_2O_3 surface sites. The formation of OH_{ads} can remove intermediates from the Pd surface by transforming the CO-like poisoning species on the surface of Pd into carbon dioxide or other cleansing products. The bifunctional mechanism occurs as follows [49−51]:

$$Co_2O_3+OH^- \leftrightarrow Co_2O_3-OH_{ads}+e \quad (2)$$

$$Co_2O_3-OH_{ads}+Pd-(CO)_{ads}+OH^- \leftrightarrow Pd+Co_2O_3+CO_2\uparrow+H_2O+e \quad (3)$$

$$Co_2O_3-OH_{ads}+Pd-(CO)_{ads}+3OH^- \leftrightarrow Pd+CO_3^{2-}+Co_2O_3+2H_2O+e \quad (4)$$

Third, the 3D nanoporous structure with more exposed Pd atoms can offer a large amount of active sites in electrolyte solutions; thus, methanol molecules can be adsorbed. The structure is favorable for the unlimited transport of molecules and electron conductivity and also favors the diffusion of intermediates, therefore enhancing the stability of the catalyst and poison resistance. In addition, compared with np-Pd, np-Pd/Co_2O_3 composites have a more refined 3D nanoporous structure and more active sites (Fig. 2, Table 2, Fig. 4 and Fig. 8), which are beneficial to enhancing the electrochemical activity.

With the increase of the Co content in the precursor alloy, the BET surface areas (Table 2) and EASAs (Fig. 8) of the np-Pd/Co_2O_3 composites made from the dealloyed Al−Pd−Co precursors (with Co existing as Co_2O_3 in composites) become larger than those of np-Pd, which is beneficial to the improvement of the catalytic activity. Furthermore, the electronic modification effects between Pd and Co as well as the synergistic effects between Pd and Co_2O_3 are also favorable for methanol oxidation, as previously mentioned. Thus, as the Co (Co_2O_3) content increases, the electrochemical activity of the composites increases. When the Co molar fraction x in the precursor is 0.5, the electrochemical activity of the np-Pd/Co_2O_3-2 composite made from dealloyed $Al_{84.5}Pd_{15}Co_{0.5}$ alloy reaches its maximum value (Figs. 9 and 10). When the Co content increases too much (x>0.5) in the precursor alloy, the nanoporous structures of the composites tend to slightly coarsen, resulting in the

reduction of the BET surface area (Table 2) and EASA (Fig. 8), which inhibits the enhancement of catalytic activity (Figs. 9 and 10). Moreover, excessive Co_2O_3 may aggregate and cover the active surface of the nanoporous structure. Under those circumstances, methanol molecules are unable to access the active sites located in the interior nanopores. As a result, the best additive content of Co in the $Al_{85-x}Pd_{15}Co_x$ precursor alloy is x=0.5.

4 Conclusions

1) 3D nanoporous Pd/Co_2O_3 composites are fabricated from the ternary Al−Pd−Co precursor alloy by facile one-step dealloying in an alkaline solution, and their composition can be controlled well.

2) All of the composites have electrocatalytic activity and long-term stability for methanol oxidation that is superior to those of np-Pd. Among these composites, the np-Pd/Co_2O_3-2 composite made from dealloying of the $Al_{84.5}Pd_{15}Co_{0.5}$ alloy possesses the best electrocatalytic activity, and its activity is enhanced by approximately 230% compared to np-Pd.

3) Enhancement of the electrocatalytic activity of the composites is due to the 3D nanoporous structure, electronic modification effect between Pd and Co, and bifunctional mechanism between Pd and Co_2O_3.

References

[1] PUGH D V, DURSUN A, CORCORAN S G. Formation of nanoporous platinum by selective dissolution of Cu from $Cu_{0.75}Pt_{0.25}$ [J]. Journal of Materials Research, 2002, 18(1): 216−221.

[2] THORP J C, SIERADZKI K, TANG L, CROZIER P A. Formation of nanoporous noble metal thin films by electrochemical dealloying of Pt_xSi_{1-x} [J]. Applied Physics Letters, 2006, 88(3): 033110−033110-3.

[3] DING Y, KIM Y J, ERLEBACHER J. Nanoporous gold leaf: "ancient technology"/advanced material [J]. Advanced Materials, 2004, 16(21): 1897−1900.

[4] WANG K, WEISSMÜLLER J. Composites of nanoporous gold and polymer [J]. Advanced Materials, 2013, 25(9): 1280−1284.

[5] XU H J, PANG S J, JIN Y, ZHANG T. General synthesis of sponge-like ultrafine nanoporous metals by dealloying in citric acid [J]. Nano Research, 2016, 9(8): 2467−2477.

[6] GUO D J, DING Y. Porous nanostructured metals for electrocatalysis [J]. Electroanalysis, 2012, 24(11): 2035−2043.

[7] XU C X, WANG L Q, WANG R Y, WANG K, ZHANG Y, TIAN F, DING Y. Nanotubular mesoporous bimetallic nanostructures with enhanced electrocatalytic performance [J]. Advanced Materials, 2009, 21(21): 2165−2169.

[8] GU J, LAN G X, JIANG Y Y, XU Y S, ZHU W, JIN C H, ZHANG Y W. Shaped Pt−Ni nanocrystals with an ultrathin Pt-enriched shell derived from one-pot hydrothermal synthesis as active electrocatalysts for oxygen reduction [J]. Nano Research, 2015, 8(5): 1480−1496.

[9] YI Q F, XIAO X Z, LIU Y Q. Hydrothermal synthesis of titanium-supported nanoporous palladium-copper electrocatalysts for formic acid oxidation and oxygen reduction reaction [J]. Transactions of Nonferrous Metals Society of China, 2013, 23(4): 1184−1190.

[10] KRAMER D, VISWANATH R N, WEISSMÜLLER J. Surface-stress induced macroscopic bending of nanoporous gold cantilevers [J]. Nano Letters, 2004, 4(5): 793−796.

[11] CHEN L Y, YU J S, FUJITA T, CHEN M W. Nanoporous copper with tunable nanoporosity for SERS applications [J]. Advanced Functional Materials, 2009, 19(8): 1221−1226.

[12] QIU H J, KANG J L, LIU P, HIRATA A, FUJITA T, CHEN M W. Fabrication of large-scale nanoporous nickel with a tunable pore size for energy storage [J]. Journal of Power Sources, 2014, 247(2): 896−905.

[13] LUX K W, RODRIGUEZ K J. Template synthesis of arrays of nano fuel cells [J]. Nano Letters, 2006, 6(2): 288−295.

[14] TANG Y Y, KAO C L, CHEN P Y. Electrochemical detection of hydrazine using a highly sensitive nanoporous gold electrode [J]. Analytica Chimica Acta, 2012, 711(2): 32−39.

[15] CHAE W S, GOUGH D V, HAM S K, ROBINSON D B, BRAUM P V. Effect of ordered intermediate porosity on ion transport in hierarchically nanoporous electrodes [J]. Acs Applied Materials & Interfaces, 2012, 4(8): 3973−3979.

[16] ZHANG X M, LI Y X, ZHANG H W, LIU Y. Evolution of porous structure with dealloying corrosion on gasar Cu−Mn alloy [J]. Transactions of Nonferrous Metals Society of China, 2015, 25(4): 1200−1205.

[17] WANG J P, WANG Z H, ZHAO D Y, XU C X. Facile fabrication of nanoporous PdFe alloy for nonenzymatic electrochemical sensing of hydrogen peroxide and glucose [J]. Analytica Chimica Acta, 2014, 832: 34−43.

[18] DONATUS U, THOMPSON G E, OMOTOYINBO J A, ALANEME K K, ARIBO S, AGBABIAKA O G. Corrosion pathways in aluminium alloys [J]. Transactions of Nonferrous Metals Society of China, 2017, 27(1): 55−62.

[19] DAN Z, XU B Q. Enhancement of Pt utilization in electrocatalysts by using gold nanoparticles [J]. Angewandte Chemie International Edition, 2006, 45(30): 4955−4959.

[20] NA H Y, ZHANG L, QIU H X, WU T, CHEN M X, YANG N, LI L Z, XING F B, GAO J P. A two-step method to synthesize palladium-copper nanoparticles on reduced graphene oxide and their extremely high electrocatalytic activity for the electrooxidation of methanol and ethanol [J]. Journal of Power Sources, 2015, 288: 160−167.

[21] ZHANG F X, CHEN J X, ZHANG X, GAO W L, JIN R C, GUAN N J. Simple and low-cost preparation method for highly dispersed Pd/TiO_2 catalysts [J]. Catalysis Today, 2004, 93−95(3): 645−650.

[22] YUWEN L H, XU F, XUE B, LUO Z M, ZHANG Q, BAO B Q, SU S, WENG L X, HUANG W, WANG L H. General synthesis of noble metal (Au, Ag, Pd, Pt) nanocrystal modified MoS_2 nanosheets and the enhanced catalytic activity of Pd-MoS_2 for methanol oxidation [J]. Nanoscale, 2014, 6(11): 5762−5769.

[23] CAO S, XU W C, ZHU S L, LIANG Y Q, LI Z Y, CUI Z D, YANG X J, INOUE A. Synthesis of TiO_2 nanoparticles loaded Pd/CuO nanoporous catalysts and their catalytic performance for methanol, ethanol and formic acid electro-oxidations [J]. Journal of The Electrochemical Society, 2016, 163(9): 263−271.

[24] ZHANG X, ZHANG Y C, ZHANG J W, ZHANG B. Anchoring ternary CuFePd nanocatalysts on reduced graphene oxide to improve the electrocatalytic activity for the methanol oxidation reaction [J]. Rsc Advances, 2015, 5(123): 101563−101568.

[25] LI G J, LU F F, WEI X, SONG X P, SUN Z B, YANG Z M, YANG S. Nanoporous Ag−CeO_2 ribbons prepared by chemical dealloying and their electrocatalytic properties [J]. Journal of Materials Chemistry A, 2013, 1(16): 4974−4981.

[26] LI G J, ZHANG X L, SONG X P, SUN Z B, FENG W J. Preparation of nanoporous Ag@TiO_2 ribbons through dealloying and their electrocatalytic properties [J]. Journal of Solid State Electrochemistry, 2015, 19(4): 967−974.

[27] ZHANG X L, WEI C H, SONG Y Y, SONG X P, SUN Z B. Nanoporous Ag−ZrO_2 composites prepared by chemical dealloying for borohydride electro-oxidation [J]. International Journal of Hydrogen Energy, 2014, 39(28): 15646−15655.

[28] BALANTA A, GODARD C, CLAVER C. Pd nanoparticles for C−C coupling reactions [J]. Chemical Society Reviews, 2011, 40(10):

4973−4985.
[29] NISHIHATA Y, MIZUKI J, AKAO T, TANAKA H, UENISHI M, KIMURA M, OKAMOTO T, HAMADA N. Self-regeneration of a Pd-perovskite catalyst for automotive emissions control [J]. Cheminform, 2002, 418(6894): 164−7.
[30] WU H X, LI H J, ZHAI Y J, XU X L, JIN Y D. Facile synthesis of free-standing Pd-based nanomembranes with enhanced catalytic performance for methanol/ethanol oxidation [J]. Advanced Materials, 2012, 24(12): 1594−1597.
[31] SONG Y Y, WEI C H, ZHANG X L, WEI X, SONG X P, SUN Z B. Nanoporous Pd/TiO_2 composites prepared by one-step dealloying and their electrocatalytic performance for methanol/ethanol oxidation [J]. Materials Chemistry and Physics, 2015, 161: 153−161.
[32] ZHANG Z H, WANG Y, QI Z, ZHANG W H, QIN J Y, FRENZEL J. Generalized fabrication of nanoporous metals (Au, Pd, Pt, Ag, and Cu) through chemical dealloying [J]. Journal of Physical Chemistry C, 2009, 113(29): 12629−12636.
[33] GRUNTHANER P J, GRUNTHANER F J, MADHUKAR A. Chemical bonding and charge redistribution: Valence band and core level correlations for the Ni/Si, Pd/Si, and Pt/Si systems [J]. Journal of Vacuum Science & Technology, 1982, 20(3): 680−683.
[34] JENKS C J, CHANG S, ANDEREGG J W, THIEL P A, LYNCH D W. Photoelectron spectra of an $Al_{70}Pd_{21}Mn_9$ quasicrystal and the cubic alloy $Al_{60}Pd_{25}Mn_{15}$ [J]. Physical Review B: Condensed Matter, 1996, 54(9): 6301−6306.
[35] FLEISCH T H, ZAJAC G W, SCHREINER J O, MAINS G J. An XPS study of the UV photoreduction of transition and noble metal oxides [J]. Applied Surface Science, 1986, 26(4): 488−497.
[36] KIM K S, GOSSMANN A F, WINOGRAD N. X-ray photoelectron spectroscopic studies of palladium oxides and the palladium-oxygen electrode [J]. Analytical Chemistry, 1974, 46(2): 197−200.
[37] TAN B J, KLABUNDE K J, SHERWOOD P M A. XPS studies of solvated metal atom dispersed (SMAD) catalysts: Evidence for layered cobalt-manganese particles on alumina and silica [J]. Journal of the American Chemical Society, 1991, 113(3): 855−861.
[38] XU C X, WANG R Y, ZHANG Y, DING Y. A general corrosion route to nanostructured metal oxides [J]. Nanoscale, 2010, 2(2): 906−909.
[39] YI Q F, NIU F J, SUN L Z. Fabrication of novel porous Pd particles and their electroactivity towards ethanol oxidation in alkaline media [J]. Fuel, 2011, 90(8): 2617−2623.
[40] PRABHURAM J, MANOHARAN R, VASAN H N. Effects of incorporation of Cu and Ag in Pd on electrochemical oxidation of methanol in alkaline solution [J]. Journal of Applied Electrochemistry, 1998, 28(9): 935−941.
[41] PATTABIRAMAN R. Electrochemical investigations on carbon supported palladium catalysts [J]. Applied Catalysis A: General, 1997, 153(1−2): 9−20.
[42] FAN Y, LIU P F, ZHANG Z W, CUI Y, ZHANG Y. Three-dimensional hierarchical porous platinum—Copper alloy networks with enhanced catalytic activity towards methanol and ethanol electro-oxidation [J]. Journal of Power Sources, 2015, 296: 282−289.
[43] LI X, CHEN G, XIE J, ZHANG L J, XIA D G, WU Z Y. An electrocatalyst for methanol oxidation in DMFC: PtBi/XC-72 with Pt solid-solution structure [J]. Journal of the Electrochemical Society, 2009, 157(4): 580−584.
[44] XU M L. Electrocatalytic performance of Pd-Ni nanowire arrays electrode for methanol electrooxidation in alkaline media [J]. Rare Metals, 2014, 33(1): 65−69.
[45] SUN J Z, WANG Y Z, ZHANG C, KOU T Y, ZHANG Z. Anodization driven enhancement of catalytic activity of Pd towards electro-oxidation of methanol, ethanol and formic acid [J]. Electrochemistry Communications, 2012, 21(1): 42−45.
[46] HABIB M A, GLUECK D. The electrochromic properties of chemically deposited tungsten oxide films [J]. Solar Energy Materials, 1989, 18(s3−4): 127−141.
[47] DEMIRCI U B. Theoretical means for searching bimetallic alloys as anode electrocatalysts for direct liquid-feed fuel cells [J]. Journal of Power Sources, 2007, 173(1): 11−18.
[48] RUBAN A, HAMMER B, STOLTZE P, SKRIVER H L, NØRSKOV J K. Surface electronic structure and reactivity of transition and noble metals 1 [J]. Journal of Molecular Catalysis A: Chemical, 1997, 115(3): 421−429.
[49] AN H, PAN L N, CUI H, LI B J, ZHOU D D, ZHAI J P, LI Q. Synthesis and performance of palladium-based catalysts for methanol and ethanol oxidation in alkaline fuel cells [J]. Electrochimica Acta, 2013, 102(21): 79−87.
[50] LIANG Y Q, CUI Z D, ZHU S L, LIU Y, YANG X J. Silver nanoparticles supported on TiO_2 nanotubes as active catalysts for ethanol oxidation [J]. Journal of Catalysis, 2011, 278(2): 276−287.
[51] ZHOU W P, LEWERA A, LARSEN R, MASEL R I, BAHUS P S, WIECKOWSKI A. Size effects in electronic and catalytic properties of unsupported palladium nanoparticles in electrooxidation of formic acid [J]. Journal of Physical Chemistry B, 2006, 110(27): 13393−13398.

对甲醇氧化具有增强效应的三维纳米多孔 Pd/Co_2O_3 复合材料的简单制备

宋衍滟[1,2,3]，段 栋[1,2,3]，时文宇[1,2,3]，王海洋[1,2,3]，孙占波[1,2,3]

1. 西安交通大学 理学院，西安 710049；
2. 西安交通大学 教育部物质非平衡合成与调控重点实验室，西安 710049；
3. 西安交通大学 陕西省先进功能材料及介观物理重点实验室，西安 710049

摘 要：为降低贵金钯的使用量同时提高甲醇氧化的催化性能，设计了超细三维纳米多孔(np)Pd/Co_2O_3 复合材料，并通过在碱液中对熔体快淬 Al−Pd−Co 合金带进行简单的一步脱合金法合成。利用 Versa-STAT MC 工作站检测了所制复合材料在碱液中的甲醇氧化电催化活性。结果表明，所得样品的韧/孔尺寸约为 8~9 nm，Co_2O_3 均匀分布在 Pd 韧带表面。其中，通过脱合金 $Al_{84.5}Pd_{15}Co_{0.5}$ 得到的 np-Pd/Co_2O_3-2 样品性能最佳，与脱合金 $Al_{85}Pd_{15}$ 所得的 np-Pd 相比，性能提高约 230%。这主要归因于 Pd 和 Co 之间存在的电子改性效应及 Pd 和 Co_2O_3 之间的双功能机理。

关键词：纳米多孔 Pd/Co_2O_3；脱合金；Al−Pd−Co 合金；电催化性能；甲醇氧化

(Edited by Bing YANG)